Three-Dimensional Analysis of Electromagnetic Wave Propagation using Meshless Time Domain Method*)

Yoshihisa FUJITA, Taku ITOH, Hiroaki NAKAMURA[1)] and Soichiro IKUNO

Tokyo University of Technology, Hachioji 192-0982, Japan
[1)]*National Institute for Fusion Science, Toki 509-5292, Japan*

(Received 7 December 2012 / Accepted 5 March 2013)

The three-dimensional analysis of electromagnetic wave propagation using meshless time domain method is numerically investigated. The basic concept of the Meshless Time Domain Method (MTDM) is same as Finite Differential Time Domain (FDTD) method. In the discretizing process of the space, the shape function of Radial Point Interpolation Method (RPIM) is adopted. Thus, MTDM can be applied to the problem in the complex shaped domain easily. The result of computation show that the value of the damping rate decrease as the frequency increases. Moreover, the value of the damping rate depend on the shape of waveguide.

Keywords: EMF, FDTD, RPIM, Meshless Time Domain Method

DOI: 10.1585/pfr.8.2401061

1. Introduction

In the Large Helical Device (LHD), the electron cyclotron heating device is used for plasma heating. The electrical power that is made by the gyrotron system transmits to LHD by using long corrugated waveguide, and the waveguide is bent at right angles several times from the gyrotron system to LHD [1]. However, it is not clear that the shape of curvature of the waveguide or transmission gain of electromagnetic wave propagation theoretically.

Generally, Finite Differential Time Domain Method (FDTD) is employed for analyzing the electromagnetic wave propagation phenomenon [2]. However, the analytic domain must be divided into orthogonal meshes if FDTD is applied for the simulation.

As is well known that the meshless approach does not require finite elements or meshless of a geometrical structure. And various meshless approaches such as the radial point interpolation method (RPIM) have been developed [3, 4]. And these methods are applied to a variety of engineering fields and the fields of computational magnetics. Particularly, meshless approaches based on RPIM are applied to time dependent problems [5].

The purpose of the present study is to develop the numerical code for analyzing a three-dimensional electromagnetic wave propagation by using MTDM. Furthermore, the relation of the waveguide size and the wave frequency is also numerically investigated by using the numerical code.

author's e-mail: yoshi@nal.ikulab.org

*) This article is based on the presentation at the 22nd International Toki Conference (ITC22).

2. Meshless Time Domain Method

In this present study, the shape function obtained by RPIM is adopted for discretization with respect to space. In the following section, we discuss about the shape function generation and discretization of Maxwell's equation in case of three-dimension.

2.1 Shape function of RPIM

First, we scatter N nodes $\boldsymbol{x}_1, \boldsymbol{x}_2, \cdots, \boldsymbol{x}_N$ in the target domain and the boundary. We assume that the approximation function $u^*(\boldsymbol{x})$ can be expanded as follows.

$$u^*(\boldsymbol{x}) = \left[\boldsymbol{b}(\boldsymbol{x})^T, \boldsymbol{p}(\boldsymbol{x})^T\right] G^{-1} \begin{bmatrix} \boldsymbol{u} \\ \boldsymbol{0} \end{bmatrix} = \boldsymbol{\phi}(\boldsymbol{x})\boldsymbol{u}. \tag{1}$$

Here the vector $\boldsymbol{b}(\boldsymbol{x})$, $\boldsymbol{p}(\boldsymbol{x})$, $\boldsymbol{u}(\boldsymbol{x})$ and $\boldsymbol{\phi}(\boldsymbol{x})$ are defined by

$$\boldsymbol{b}(\boldsymbol{x}) = [b_1(\boldsymbol{x}), b_2(\boldsymbol{x}), \cdots, b_N(\boldsymbol{x})]^T, \tag{2}$$

$$\boldsymbol{p}(\boldsymbol{x}) = [p_1(\boldsymbol{x}), p_2(\boldsymbol{x}), \cdots, p_M(\boldsymbol{x})]^T, \tag{3}$$

$$\boldsymbol{u}(\boldsymbol{x}) = [u_1(\boldsymbol{x}), u_2(\boldsymbol{x}), \cdots, u_N(\boldsymbol{x})]^T, \tag{4}$$

$$\boldsymbol{\phi}(\boldsymbol{x}) = [\phi_1(\boldsymbol{x}), \phi_2(\boldsymbol{x}), \cdots, \phi_N(\boldsymbol{x})]^T, \tag{5}$$

where $b(\boldsymbol{x})$, $p(\boldsymbol{x})$, $u(\boldsymbol{x})$ and $\phi(\boldsymbol{x})$ denote the Radial Basis Function (RBF), the Polynomial Basis Function (PBF), expansion factor and the shape function, respectively. In the present study, $\boldsymbol{p}(\boldsymbol{x}) = [1, x, y]^T$ is adopted for monomials approximation. Furthermore, the matrix G is defined by following equation.

$$G = \begin{bmatrix} B & P \\ P^T & O \end{bmatrix}. \tag{6}$$

Here, the matrices B and P are defined by following equations.

$$B = [\boldsymbol{b}(\boldsymbol{x}_1), \boldsymbol{b}(\boldsymbol{x}_2), \cdots, \boldsymbol{b}(\boldsymbol{x}_N)]^T, \tag{7}$$

$$P = [\boldsymbol{p}(\boldsymbol{x}_1), \boldsymbol{p}(\boldsymbol{x}_2), \cdots, \boldsymbol{p}(\boldsymbol{x}_N)]^T. \tag{8}$$

Various functions are proposed for RBF [6]. In the present study, following function is adopted for RBF.

$$b(\boldsymbol{x}_i) = \left[\left(\frac{r}{R}\right)^2 + 1.0\right]^{-0.5}. \tag{9}$$

Here, R denotes a support radius of the influence domain, r is defined by $r = |\boldsymbol{x} - \boldsymbol{x}_i|$. By solving the linear system obtained from (1), the shape functions which is located on each node are derived.

The shape function obtained by above method satisfies following the Kronecker's delta function property [3], and the approximation function can be simply expressed.

$$\phi_i(\boldsymbol{x}_j) = \begin{cases} 1, & i = j, \\ 0, & i \neq j. \end{cases} \tag{10}$$

2.2 Discretization by shape function

The governing equation of the three-dimensional wave propagation phenomenon is defined by following equations.

$$\frac{\partial \boldsymbol{E}}{\partial t} = -\frac{\sigma}{\epsilon}\boldsymbol{E} + \frac{1}{\epsilon}\nabla \times \boldsymbol{H}, \tag{11}$$

$$\frac{\partial \boldsymbol{H}}{\partial t} = -\frac{1}{\mu}\nabla \times \boldsymbol{E}. \tag{12}$$

Here, $\boldsymbol{H}$ denotes a magnetic field and $\boldsymbol{E}$ denotes electric field. Moreover, ϵ, μ, and σ denote permittivity, permeability, and electro conductivity, respectively. The basic concept of MTDM is same as that of FDTD. Thus, time region is discretized by using the Leap-Frog algorithm. Note that we must be taken an account of the numerical stability condition because the Leap-Frog algorithm is explicit method. Taking account of the numerical stability condition, nodes are scattered so as to satisfy the following equation.

$$v\frac{\Delta t}{\min\limits_{i \neq j} |\boldsymbol{x}_i - \boldsymbol{x}_j|} \leq 1. \tag{13}$$

Here, v denotes a wave speed and Δt denotes a step size of time. On the other hand, the space is discretized by using the shape function obtained by RPIM. The shape function obtained by RPIM has the Kronecker's delta function property, and the approximation function can be expressed briefly. Finally, following discretized equations are derived.

$$E^n_{x,m} = \alpha\left[\left(\frac{\epsilon}{\Delta t} - \frac{\sigma}{2}\right)E^{n-1}_{x,m} + \sum_i H^{n-\frac{1}{2}}_{z,i}\frac{\partial \phi_i}{\partial y} - \sum_i H^{n-\frac{1}{2}}_{y,i}\frac{\partial \phi_i}{\partial z}\right], \tag{14}$$

$$E^n_{y,m} = \alpha\left[\left(\frac{\epsilon}{\Delta t} - \frac{\sigma}{2}\right)E^{n-1}_{y,m} + \sum_i H^{n-\frac{1}{2}}_{x,i}\frac{\partial \phi_i}{\partial z} - \sum_i H^{n-\frac{1}{2}}_{z,i}\frac{\partial \phi_i}{\partial x}\right], \tag{15}$$

$$E^n_{z,m} = \alpha\left[\left(\frac{\epsilon}{\Delta t} - \frac{\sigma}{2}\right)E^{n-1}_{z,m} + \sum_i H^{n-\frac{1}{2}}_{y,i}\frac{\partial \phi_i}{\partial x} - \sum_i H^{n-\frac{1}{2}}_{x,i}\frac{\partial \phi_i}{\partial y}\right], \tag{16}$$

$$H^{n+\frac{1}{2}}_{x,m} = H^{n-\frac{1}{2}}_{x,m} + \frac{\Delta t}{\mu}\left(\sum_i E^n_{y,i}\frac{\partial \phi_i}{\partial z} - \sum_i E^n_{z,i}\frac{\partial \phi_i}{\partial y}\right), \tag{17}$$

$$H^{n+\frac{1}{2}}_{y,m} = H^{n-\frac{1}{2}}_{y,m} + \frac{\Delta t}{\mu}\left(\sum_i E^n_{z,i}\frac{\partial \phi_i}{\partial x} - \sum_i E^n_{x,i}\frac{\partial \phi_i}{\partial z}\right), \tag{18}$$

$$H^{n+\frac{1}{2}}_{z,m} = H^{n-\frac{1}{2}}_{z,m} + \frac{\Delta t}{\mu}\left(\sum_i E^n_{x,i}\frac{\partial \phi_i}{\partial y} - \sum_i E^n_{y,i}\frac{\partial \phi_i}{\partial x}\right). \tag{19}$$

Here, the parameter α is defined by following equation.

$$\alpha = \frac{1}{\dfrac{\epsilon}{\Delta t} + \dfrac{\sigma}{2}}. \tag{20}$$

Moreover, the superscript of the variables denotes a time step, and the subscripts of the variables denote a component and a node number. Solving equations (14), (15) and (16) by using a initial condition, the value of electric field is obtained. Substituting the calculated values of electric field to equations (17), (18) and (19) the value of magnetic field is obrained. These equation alternately calculated, and the time dependent behavior can be calculated.

3. Numerical Evaluations

In the present study, two types of waveguide are adopted for the numerical evaluation, and the values of damping rate are calculated by means of the numerical code. The value of damping rate R_{D} used in this study is defined by following equation.

$$R_{\mathrm{D}} = \frac{\left\langle \int_{\Omega_{\mathrm{out}}} E\, d\Omega \right\rangle_t}{\left\langle \int_{\Omega_{\mathrm{in}}} E\, d\Omega \right\rangle_t}. \tag{21}$$

Here, E is defined by $E = E_x^2 + E_y^2 + E_z^2$ and $\langle x \rangle_t$ denotes a time average of x. Ω_{in} and Ω_{out} denote a cross-section of the waveguide as shown in Figs. 1, 5. Furthermore, the Perfectly Matched Layer (PML) and the Perfect Electric Conductor (PEC) are adopted for absorbing boundary condition and boundary condition. PMLs are imposed at edges of waveguide and PECs are imposed on side of the waveguide. (see Figs. 1, 5). The parameters that used in this study are also shown in Table 1. Note that the value of support radius R is determined a number of nodes contained inside of influence domain are to be 12.

3.1 Cuboid waveguide

Let us first investigate the wave propagation phenomenon in the cuboid waveguide by means of MTDM,

Table 1 Physical parameters for the calculation. Here λ denotes a wavelength.

Input Wave	Sine Wave
Amplitude	1.0 [V/m]
Frequency	15.0 [GHz]
Wave speed	3.0×10^8 [m/s]
Distance of neighboring node	$20/\lambda$
Number of layer for PML	16
Dimension of PML	4
Reflectance factor of PML	−80 [dB]

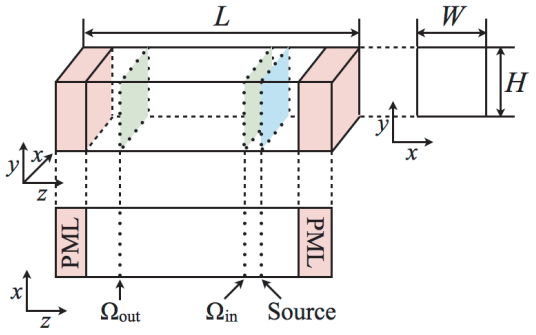

Fig. 1 Conceptual diagram of the rectangular waveguide.

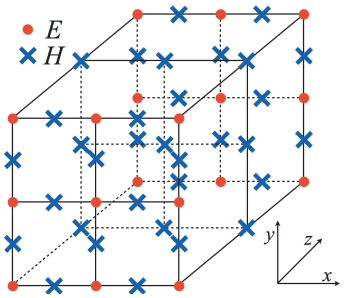

Fig. 2 The node alignment of the electric field and the magnetic field in the cuboid.

and the values of damping rate are numerically evaluated. The evaluation target is the cuboid waveguide, and the conceptual diagram of the analytic model is shown in Fig. 1. In addition, the node alignment of the electric field $\boldsymbol{E}$ and the magnetic field $\boldsymbol{H}$ is shown in Fig. 2. The node alignment of the electric field and the magnetic field is designed on the basis of staggered mesh that used in standard FDTD. The distribution of E_z in the cuboid waveguide is shown in Fig. 3.

The values of damping rate R_D in the cuboid waveguide are plotted as a function of the width and height of waveguide in Fig. 4. We see from this figure that the value of R_D decrease as the frequency increases in both cases. It can be also seen from the figure that the reduction of R_D is remarkable in case of 30 [GHz]. In other words, low frequency is hardly affected by the shape of waveguide.

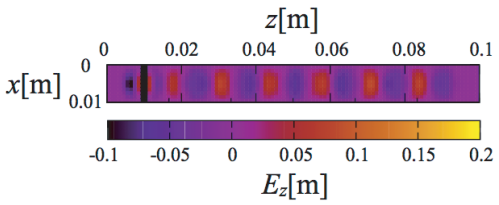

Fig. 3 The distribution of E_z in the cuboid waveguide in case of $L = 0.1$ [m], $W = 0.01$ [m], $H = 0.01$ [m].

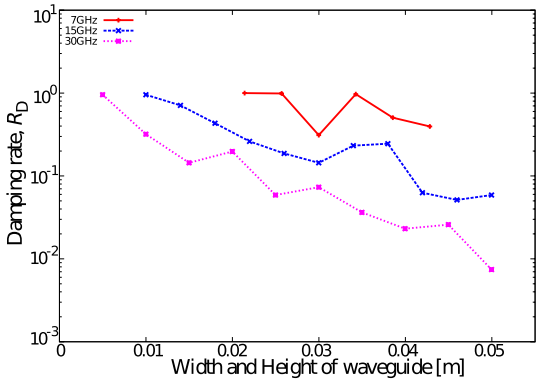

Fig. 4 The values of damping rate R_D are plotted as a function of the width W and height H of waveguide. Note that the value of L is fixed as $L = 0.2$ [m], and the values of W, H are satisfied $W = H$.

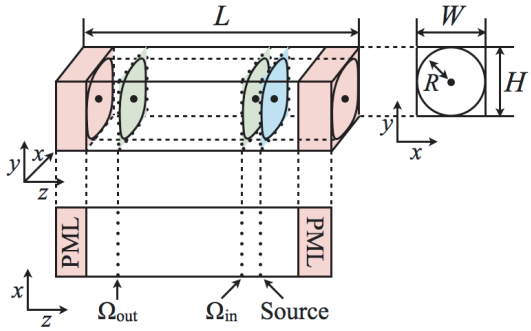

Fig. 5 Conceptual diagram of the cylinder.

3.2 Cylinder waveguide

Next, we investigate the wave propagation phenomenon in the cylinder waveguide. The conceptual diagram of the evaluation target is shown in Fig. 5. The node alignment of the electric field $\boldsymbol{E}$ and the magnetic field $\boldsymbol{H}$ is also shown in Fig. 6. The cross-section of the analytic region of waveguide is the area circle inscribed in a square area (see Fig. 5). The distribution of E_z in the cylinder waveguide is shown in Fig. 7. We can see from this figure that the distribution of E_z in the cylinder waveguide is different from that of cuboid waveguide. This is because the shape of the wave is changed by the reflection at the corner of the cuboid waveguide. On the other hand, the effect of the reflection decrees by the shape of waveguide in case of cylinder waveguide.

Finally, we evaluate the values of damping rate R_D in

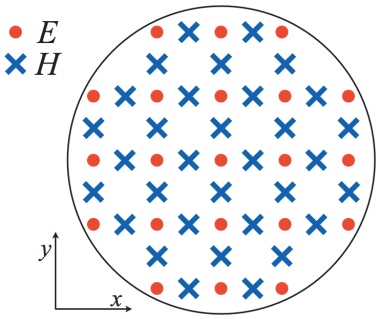

Fig. 6 The node alignment of the electric field and the magnetic field in the cylinder.

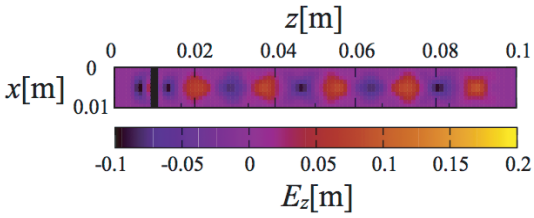

Fig. 7 The distribution of E_z in the cylinder in case of $L = 0.1$ [m], $W = 0.01$ [m], $H = 0.01$ [m].

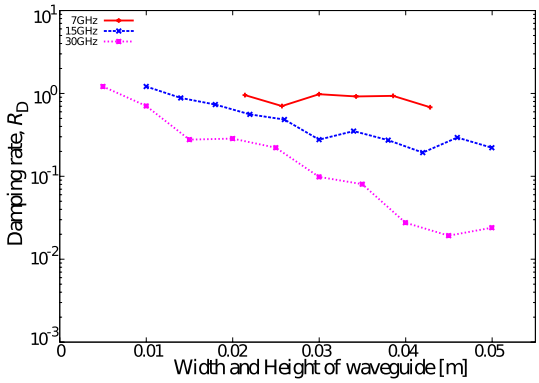

Fig. 8 The values of damping rate R_D are plotted as a function of the width and height of waveguide. Note that the value of L is fixed as $L = 0.2$ [m], and the values of W, H are satisfied $W = H$.

the cylinder waveguide, and the values of R_D are plotted as a function of the width and height of waveguide in Fig. 8. We see from this figure that the value of R_D decrease as the frequency increases in both cases. This behavior is almost same as that of cuboid waveguide. However, the behavior of decreasing in cylinder waveguide is found to be smoother compared to the behavior of cuboid waveguide. This is considered to be result of the influence of the reflection.

4. Conclusion

We have developed the numerical code for three-dimensional analysis of electromagnetic wave propagation by using MTDM. By using the code, the influence of waveguide's shape on damping rate.

Conclusions obtained in the present study are summarized as follows.

- The values of R_D decrease as frequency increases in case of cuboid waveguide and cylinder waveguide.
- The decreasing phenomenon of the damping rate showed in Fig. 4 and Fig. 8 can be explained as follows. The values of damping rate are almost same if the values are plotted as a function of λ/L. That is to say, the value of damping rate depend on the λ and size of width and height of waveguide. In addition, the optimal size of width and height of waveguide is $\lambda/2$.
- The behavior of decreasing in cylinder waveguide is found to be smoother compared to the behavior of cuboid waveguide. Because the length of the radial is constant in cylinder waveguide. On the other hand, the length of the radial is non-constant in cuboid waveguide, and the propagation behavior is affected by reflection from the edge of the waveguide. From these reasons, the distribution of the electric field in cylinder waveguide is more smooth than that of cuboid waveguide.
- On the whole, linear waveguide should be cylinder waveguide.

Acknowledgment

This work was supported in part by Japan Society for the Promotion of Science under a Grant-in-Aid for Scientific Research (B) No.22360042. A part of this work was also carried out under the Collaboration Research Program (No.NIFS09KDBN003) at National Institute for Fusion Science, Japan.

[1] S. Yamada, T. Mito, H. Chikaraishi, S. Tanahashi, S. Kitagawa, J. Yamamoto and O. Motojima, IEEE Trans. Mag. **32**(4), 2422 (1996).
[2] K. Yee, IEEE Trans. Annt. **14**(3), 302 (1966).
[3] J.G. Wang and G.R. Liu, Int. J. Numer. Methods Eng. **54**(11), 1623 (2002).
[4] T. Belytschko, Y.Y. Lu and L. Gu, Int. J. Numer. Methods Eng. **37**(2), 229 (1994).
[5] T. Kaufmann, C. Fumeaux and R. Vehldieck, IEEE Trans. Microw. Theory Tech. **58**(12), 3399 (2010).
[6] S. Ikuno, Y. Fujita, T. Itoh, S. Nakata, H. Nakamura and A. Kamitani, J. Plasma Fusion Res. **7**, 2406044 (2012).